Current Applied Science and Technology Vol. 21 No. 2 (April-June 2021)

Dong Ra Nang National Forest Change Detection using Multi-temporal LANDSAT 7 ETM$^+$ Imagery by Using CART Classification: Object-Oriented Approach

Sopholwit Khamphilung*

Department of Geoinformatics, Faculty of Informatics, Mahasarakham University, Maha Sarakham, Thailand

Received: 25 May 2020, Revised: 8 September 2020, Accepted: 12 November 2020

Abstract

This study presents change detection analysis using object-based image analysis in Dong Ra Nang national forest, Kalasin province. This national forest was previously cleared and used for agricultural purposes for an extended period of time according to media reports published between 2007-2015. In order to perform a LU/LC examination, a time series of LANDSAT 7 ETM$^+$ images acquired from 3 dates (25/11/1999, 28/11/2007 and 21/11/2015) were used for image segmentation and LU/LC classification. Furthermore, a CART algorithm and crucial image band ratios, such as MSAVI and NDVI, including mean of image layer bands, were used to improve image classification of degradation of the forest. The information from three thematic layers sampling points that had been derived from visual interpretations was used for CART training, applying and classifying the satellite images into 6 LU/LC classes, namely, (1) dense forest, (2) light forest, (3) bare land, (4) agricultural area, (5) plantation area, and (6) bodies of water on hierarchical image networks. Prior to the deforestation detection analysis, each image scene was classified individually using a CART algorithm. Then, the classified images were synchronized with the main map for performing land use/ land cover changes analysis focused on deforestation using image hierarchical image network by relation to image objects in vertical and horizontal aspects. The results indicated that the forest areas decreased dramatically by 50% from 1999-2007. On the other hand, there was a slight increase in bare land by an area of 38.68 sq.km. The majority of the area was used for farm land according to the report of the Forest Management Office, Khon Kaen province. The vegetation area emerged in the central area surrounding by bare land and agricultural area. In 2007-2015, the vegetation rapidly decreased by 30.89 sq.km., and the area tended to be bare land and agricultural area.

Keywords: OBIA; remote sensing; classification and regression tree; CART
DOI…….

*Corresponding author: Tel.: (+66) 85-5503-666, Fax: (+66) 43-3547-59
E-mail: sopholwit.c@msu.ac.th

1. Introduction

National forests play an important role in social and economic aspects of the country. Dong Ra Nang is a well-known national forest located in the rural districts of Kalasin Province, Northeast, Thailand. There are issues of forest encroachment by villagers who live around the forest area. Their searching for subsistence plants, farming and logging have led to deforestation in the forest. The rainforest has the potential to develop a significant biodiversity. Therefore, the forest should be protected from unexpected phenomena, especially illegal natural resources over-exploitation. Interestingly, the forest is home to many important economic trees, such as Teak wood, Agar wood, and Yang. In terms of land use/land cover change detection, various processes can be used to study land use/land changes, particularly the process of remote sensing classification techniques or field surveying. Earth Observation Satellites (EOS) are emerging in various systems and image resolution; such as LANDSAT satellite imagery. The researcher was able to compare those imageries in the same area from past to present based on existing temporal resolution from selected data sources. In image classification; however, satellite imagery is characterized by two types of classification procedures, namely, pixel-based and object-based image analysis [1, 2]. The similarity of this methodology is that some advantage of spectral information derived from various sensors, can comply with statistical analysis tools (i.e. Parallelepiped, Maximum likelihood classifier) [3, 4]. Pixel-based image analysis has the disadvantage that it cannot take the spatial relations among target pixels, for example, the distance between objects, sizes, and shape information aimed at integrating to the target classes [5]. Such crucial information can be the criteria that make image classification more accurate. Object-based image analysis, on other hand, is more likely to overcome some of the drawbacks from the previously-mentioned image classification approach. In addition, pixel-based image analysis also shows a classification result error called the salt and pepper effect. Since pixel-based image classification is focused on individual pixels without considering the spatial relationships among the image objects, one pixel can be classified in more than one class. Generally, objects on the Earth's surface are categorized into two main types. i.e., man-made and natural features observing from satellite imageries. Visual interpretation and digital image processing can be used to distinguish image features. Some land covering objects, such as bodies of water, agricultural areas are involved not only because of their spectral information but also because of their shape characteristics (e.g., compactness, rectangular fit and roundness). These shape properties are derived from the image segmentation from the pixel homogeneity values by comparison with size and shape [6, 7]. However, these objects can be discriminated by an experienced user who can recognize some emerged shape, such as geometry of natural bodies of water, and man-made bodies of water with different shapes. In term of digital satellite image analysis, object-based image analysis is able to involve spectral and geometric information for classification procedures that increase classification quality. Moreover, object-oriented analysis comprises optimal tools and algorithms that can increase the accuracy and precision of image classification more than any other classifier paradigms can. For this research, a CART Algorithm was applied to identify the changes in LU/ LC classification focusing on forest changes [6-8]. Obviously, object-based image analysis applied to VHR imagery [9], and modification of LU/LC change detection by utilizing object-oriented approach have become more and more popular approaches for satellite image classification. Furthermore, pixel-based and object-based image analysis for change detection were also compared to see which could provide the best solution in a particular area [10].

2. Materials and Methods

2.1 Study area and data

This study utilized LANDSAT 7 ETM$^+$ images that were acquired on November 25, 1999 / Nov 28, 2007/ and November 21, 2015 which had spatial resolution 30 x 30 meters by the use of the object-oriented approach (Figure 1). Prior to classification, pre-processing of the data was performed, such as image subset creation, image filtering and geo-referencing for data quality improvement. Based on the various satellite image bands; set-relevant and appropriate bands were selected for data analysis. The utilized multispectral bands revealed the target objects reflectance, e.g., near infrared (NIR), which has the characteristic of reflecting the vegetation information. It can be used for performing of image band ratios, such as Normalized Difference Vegetation Index (NDVI). This research employed 4 bands of LANDSAT 7 ETM$^+$ images, namely, ETM$^+$ band 1 (Blue band: 0.450-0.515 μm), ETM$^+$ band 2 (Green band: 0.525-0.605 μm), ETM$^+$ band 3 (Red band: 0.630-0.69 μm), and ETM$^+$ band 4 (NIR band: 0.775-0.900 μm), respectively (Table 1).

2.2 Image segmentation

Image segmentation is one the most important processes aimed at creating image objects from various pixel values. Optimal scale parameters were derived from multiresolution segmentation algorithm evaluated using ESP Tools (Estimate Scale Parameter) [11, 12]. This algorithm merges candidate adjacent pixels to the best fit image objects from user defined criterion. The process starts by searching an image pixel and merging a nearest neighbor repeatedly creating image objects based on spectral and shape homogeneity criterion defined by the user [13, 14]. Each image was segmented for creating image objects using scale parameter = 15, shape = 0.2, and compactness = 0.7, respectively (Table 2). Hierarchical image object level L1T1 represents the initial image object level 1 derived from LANDSAT 7 ETM$^+$ imagery acquired on November 25, 1999. Hierarchical image object levels L1T2 and L1T3 refer to the next two years of dynamic circumstances in the preservation area, i.e. year 2007 and 2015. Image layer weight was used to emphasize the most important target values assigned to NIR band with a layer weighted value of 3, which was aimed at the emphasis of vegetative reflectance, while other image bands weighted with value of 1. The appropriate factors for determination for image object level 1 were derived by computing a statistical value algorithm to obtain the optimal correlation values. Each image was copied to create new image object level that represents dynamic time series for possibility changes, including image hierarchical network properties applying to each image year. There are 3 new image object levels containing processed data that are prepared for individual LU/LC classification by CART classifier.

2.3 Feature analysis and selection

Prior to creating the rule set for classification, feature analysis is performed from various spectral and contextual information [15]. Spectral information; for example, image mean layers (mean Blue, mean Green, maen Red and mean NIR) are used as the image objects reflectance from certain classes. Contextual information describes shape characteristics and spatial relations of image objects related to man-made and natural features. Thus, this paper considers crucial integration factors to discriminate forest and non-forest area without considering social factors. Moreover, the modified

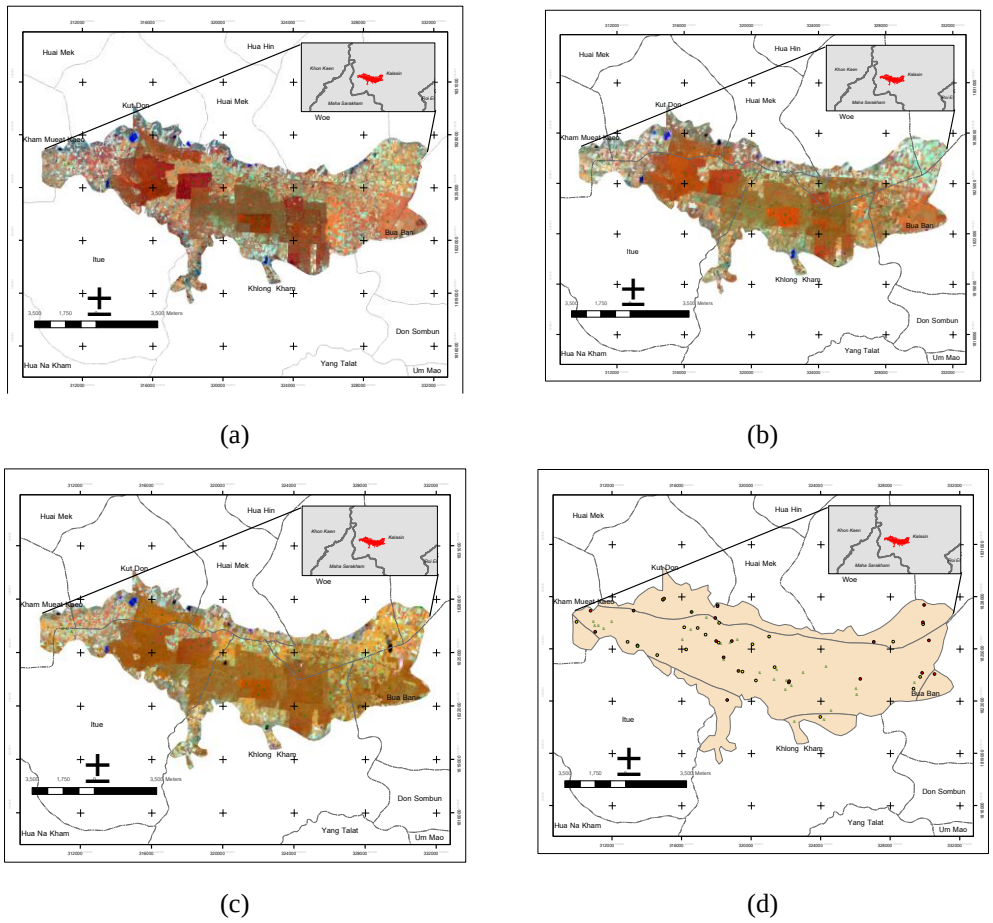

Figure 1. (a) LANDSAT 7 ETM$^+$ R,G,B 4,5,3 acquired on 25/11/1999, (b) LANDSAT 7 ETM$^+$, R,G,B 4,5,3 acquired on 28/11/2007, (c) LANDSAT 7 ETM$^+$, R,G,B 4,5,3 acquired on 21/11/2015, and (d) sampling plots from visual interpretation

Table 1. Image bands selection and alias names

Date	Bands	Alias Names
25/11/1999	Mean Blue, Mean Green, Mean Red, Mean NIR	1999_Blue, 1999_Green, 1999_Red, 1999_NIR
28/11/2007	Mean Blue, Mean Green, Mean Red, Mean NIR	2004_Blue, 2007_Green, 2007_Red, 1999_NIR
21/11/2015	Mean Blue, Mean Green, Mean Red, Mean NIR	2015_Blue, 2015_Green, 2015_Red, 2015_NIR

Table 2. Multiresolution image segmentation properties

Date	Scale parameter	Shape	Compactness	Image Layer weight	Image Object Level	Image objects
25/11/1999	15	0.2	0.7	Blue=1,	L1T1	2,383
28/11/2007	15	0.2	0.7	Green=1,	L1T2	1,576
21/11/2015	15	0.2	0.7	Red =1, NIR=3	L1T3	4,212

soil-adjusted vegetation index (MSAVI) was used for improving forest area and soil reflectance classification in areas that some indices were not able to carry out an appropriate result. This index seeks to address the limitations of NDVI and has been applied to areas with high reflectance of soil surface [16]. The output of MSAVI is a new image layer represents vegetation greenness with values ranging from -1 to +1 (equation 1).

$$\boldsymbol{MSAVI} = \frac{(\boldsymbol{NIR} - \boldsymbol{RED})(\mathbf{1}+\boldsymbol{L})}{\mathbf{NIR}+\mathbf{RED}+\mathbf{L}} \quad (1)$$

More interestingly, when apply this index, L value is the soil-brightness correction factor that needs to be input to the equation. L value is usually calculated from NIR and RED bands from selected data multiplied by 2 and s factors. However, users are able to choose the default value of 0.5 instead of using the calculation equation (equation 2).

$$\boldsymbol{L} = \frac{\mathbf{2}*\mathbf{s}*(\mathbf{NIR}-\mathbf{RED})*(\mathbf{NIR}-\mathbf{s}*\mathbf{RED})}{\mathbf{NIR}+\mathbf{RED}} \quad (2)$$

The results of the CART classification were derived from the multi-temporal imageries, and then these were examined by combining several processes to figure out the increase and decrease of forest and non-forest area. Fields surveys were verified using GPS, including the reference points and the relevant reference image objects collected from well-known target area. In order to determine the percentage of post-classification accuracy, the goal of overall accuracy should be 80 percent or higher.

2.4 Classification and regression tree (CART)

In this paper, satellite imageries were classified by using CART algorithm [17, 18]. Prior to that achievement, 3 points sample data sets were derived from visual interpretation which represented training areas for each LU/LC class by cognition domain input to the algorithm. Each point layer was created individually based on the target LU/LC classes that emerged from the study area. The vector data contained spatial and attribute information in point data representation model. There were 31 visual interpretation classified points corresponding with 6 classes in 1999, 20 points for 2007, and 25 points in 2015. The image objects data inherited image objects information from image segmentation and image selected bands, such as mean image band information and some image band ratios, such as NDVI, etc. The CART classifier comprises training, applying, querying, and authentication after classified. The training process as described above is based on classified points defined by visual interpretation, including the selected image features information. The CART (classification and regression tree) is non-parametric classification rule [19, 20]. The algorithm begins with creating a non-terminal binary tree node for each single input variable (x), and then splits this node with max purity with Gini index recursive process creating next two child nodes. The leaf nodes of the tree contain an output variable (y) which is used to make a prediction. The

process continues dividing tree branches until every aspect of the dataset is classified and visible in tree leaf nodes. For example, a classification node t_1 is a starting node for dividing dataset on x-y plane into two groups, i.e., t_2 and t_3. Then, t_2 and t_3 can represent the next terminal nodes for the classification possible class until a suitable tree is constructed.

2.5 Image classification

2.5.1 Data preparation

Prior to image classification by CART algorithm, there were 3 point vector layers created from visual interpretation for LU/LC data input into the model as described above. Each layer covered all of the target land use/land cover classes in 3 specific time series used for training CART, including spectral information and contextual information of selected classes.

2.5.2 Applying CART algorithm

There are 4 processes of decision tree classification, namely, vector to sample, training, applying and querying from unknown image objects to the target classes [21, 22]. Each imagery is input to the algorithm for creating the new classes from the visual interpreted point data using the assign class by thematic layer and vector to sample algorithms. The target class classified from the thematic layer 1 inherits attribute information from the attribute data (field name *Class_name)*, which maintain corresponding LU/LC classes for hierarchical image network level L1T1. Then, this classified layer was input to training process employing image object properties and selected features to determine what nodes, branches and child nodes should be constructed on the decision tree diagram. There were 7 object features used in the multiple features selection on image object level L1T1 and on the mapT1 (1999), namely, MSVI, NDVI and layer mean Green, mean Blue, mean Red, and mean NIR derived from each year. In the classification process, the system requirements properties were set for creating classification tree nodes and branches to achieve the optimum results. The maximum tree depth was set to 9, the minimum number of samples per node = 2, possible cluster values of a categorical variable = 16, and performance of cross validation = 3. Then, these properties were applied to the mapT2 (2007), and the mapT3 (2015) for creating and classifying the image object layers L2T2 and L3T3, respectively. The 3 image time series were analyzed in the same environment using CNL (Cognition Network Language) employed in object-based image analysis workflow creating the classification rule set [23]. The query process illustrates CNL tree on the specific location enabled branches and nodes classified from above described properties. The results show both LU/LC maps and arcs/nodes generated from CART algorithm.

2.5.3 Accuracy assessment

This process was performed from individual data examined from points, image objects and field random check points and verified by GPS in the study area. The existing collected points were compared with the visual classified images, including the existing maps as described above. This process was performed on each year's data based on existing and training information, including sample image objects derived from visual interpretation used as TTA masks. The target classes were evaluated from error matrix focused on user's accuracy and producer's accuracy and calculated for overall accuracy and kappa statistics. This research set a goal for overall accuracy of the image classification in each year at more than 80%.

2.5.4 Land use/land cover change evaluation using hierarchical image network

The classified images were evaluated using image object hierarchical networks from vertical and horizontal aspects [24, 25]. Each independent classified map was synchronized to the main map that represented the initial state for all analytical tasks [26]. Change detection was evaluated using image objects correlation from all directions based on existing classified image objects from image temporal resolution, including class descriptions from the class hierarchy approach [27]. The main map stands for the start and end points from the first step of the study till the achievement of changes evaluation [28]. This map layer comprises 3 maps collected from all transformative results from the classified independent maps, i.e. mapT1, mapT2 and mapT3 [29]. Change detection technique utilized the hierarchical image network to compare by relation to image objects on the horizontal X-axis, and by correlation to sub-objects on the vertical aspect (Y-axis) [30, 31]. The analytical processes are illustrated in Figure 2.

3. Results and Discussion

3.1 Image classification

The Landsat 7 ETM^+ imageries were classified using object-oriented approach in Dong Ranang national forest, Kalasin province, Thailand from 1999-2015, as described above. The 1999 image classification results show that the 6 target classes were spread throughout the area (Figures 3 and 4). The initial node had a 100% brightness value (<64.82), and in the next two child nodes, the brightness was divided into 59.3% of mean 1999_blue layer classified as light forest, and brightness of 48%.1% was classified as light forest. MSVIT1 information inherited at 37% was separated into 18.5% classified as dense forest, and the next node still had MSVIT1 of less than 0.783, which was classified as light forest (7.4%) and dense forest (11.1%). On the first right node classified to brightness and mean 1999_blue spectral information. The brightness < 76.76 divided to plantation area and agricultural area, and the 1999_blue < 79.81 was classified as bare land and body of water. The largest area identified was plantation area, which occupied 50.57 sq.km, followed by agricultural area at 17.54 sq.km, and body of water at 4.32 sq.km. (Table 3).

In 2007, the mean layer of blue band value was the initial point with a value of <73.93 (100%). The next two branches inherited brightness with < 60.38 (50%) and 50% of mean 2007 NIR (< 52.41). The brightness value divided into a 2007_green value node, classified as plantation area (Figures 5 and 6). The 2007_green information classified to dense and light forest. The mean 2007_NIR information scored <51.41 (50%) and classified to body of water at the first right node, and the next node displayed mean brightness value of < 74.45, and classified to agricultural area and bare land with mean brightness of 15% and 25%, respectively. Dense forest was absent in this year. Agricultural area was the main land cover class by 46.97 sq.km., followed by light forest 20.14, plantation area 11.86, and 0.77 sq.km was body of water (Table 4).

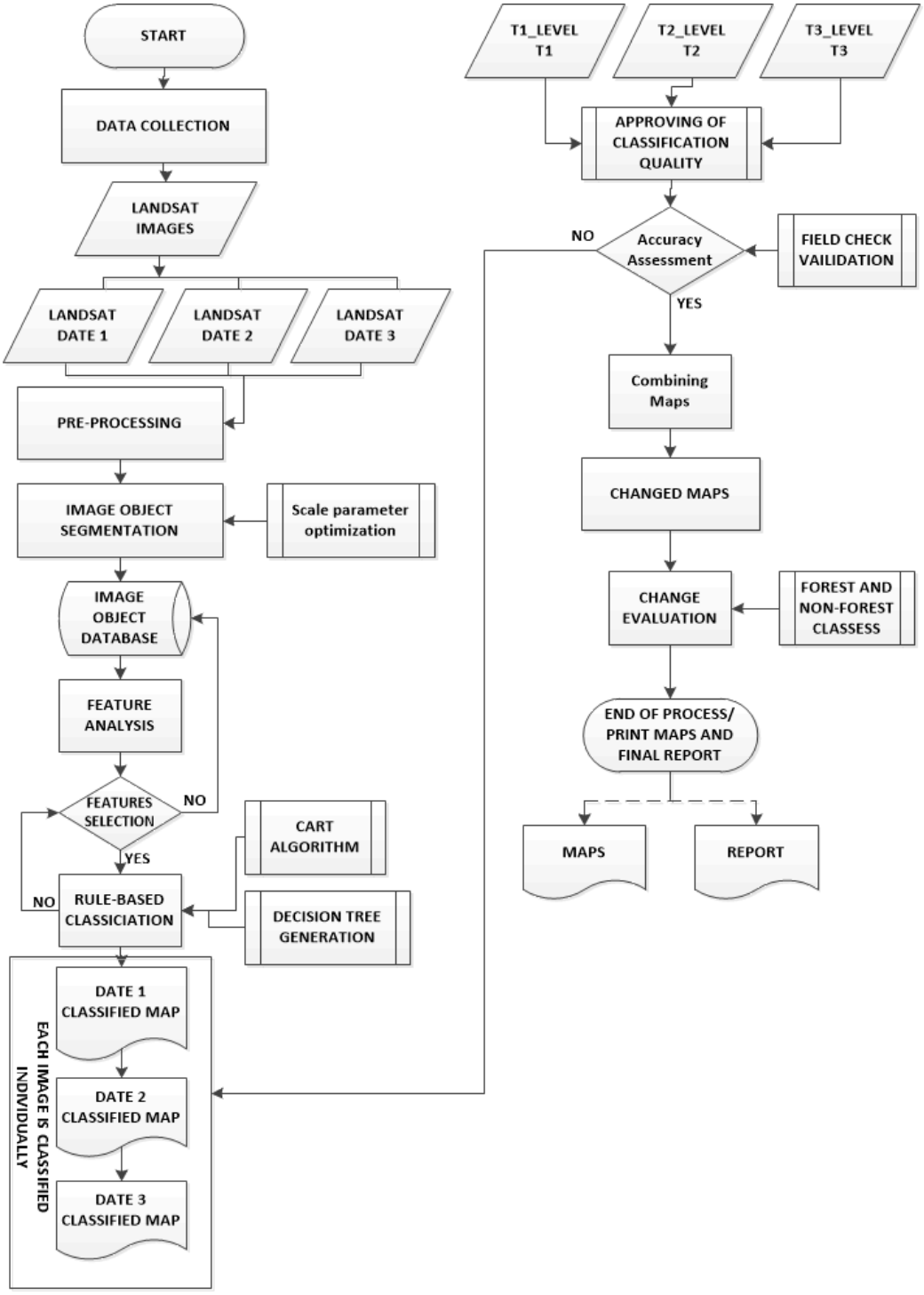

Figure 2. Workflow diagram of Dong Ranang change detection analysis

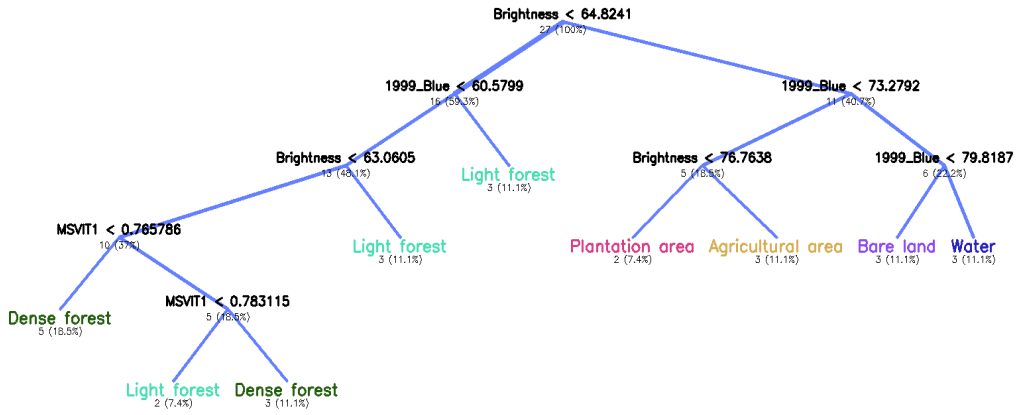

Figure 3. CART parent and child nodes in 1999

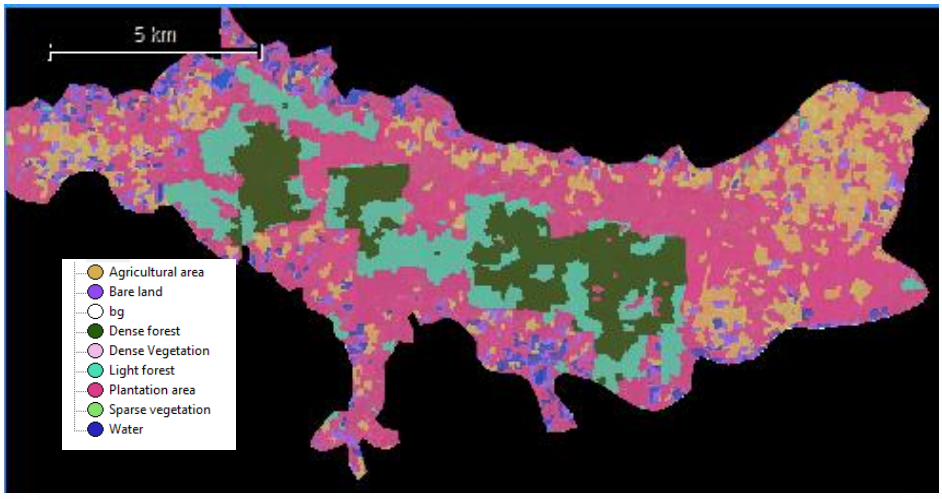

Figure 4. LANDSAT 7 ETM^{+} imagery classification result in 1999

Table 3. The classification area in 1999

Class name	Area (sq.km)
Dense forest	13.88
Light forest	14.70
Agricultural area	17.54
Bare land	5.88
Plantation area	50.57
Water body	4.325
Total	**106.89**

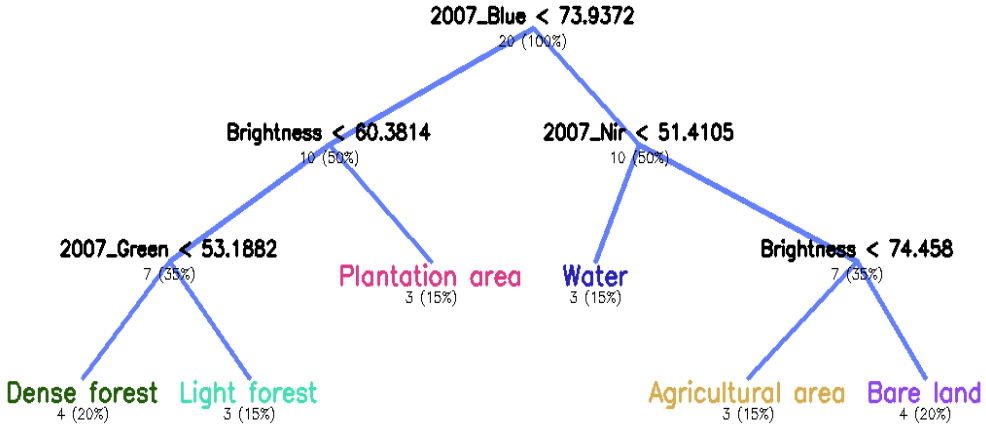

Figure 5. CART parent and child nodes in 2007

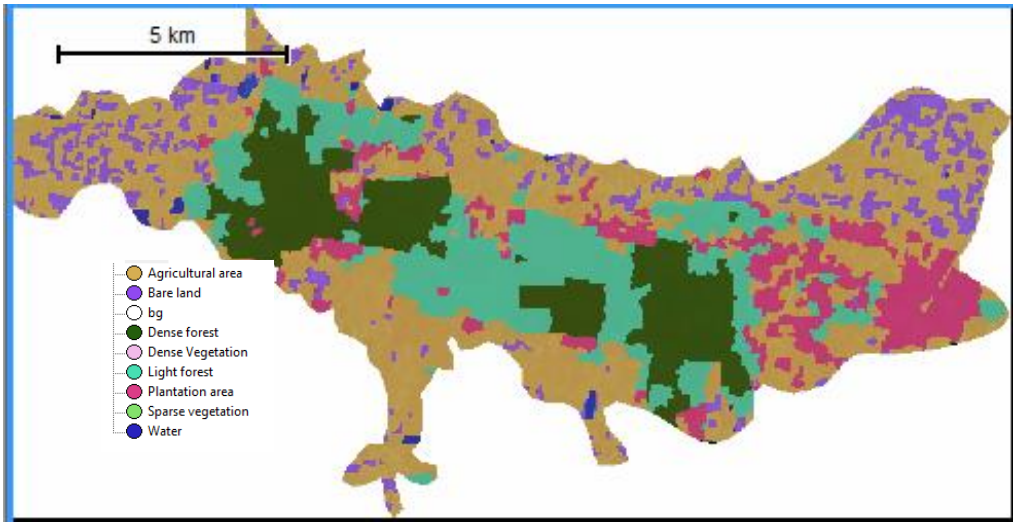

Figure 6. Landsat 7 ETM^{+} imagery classification result in 2007

Table 4. The classification area in 2007

Class name	Area (sq.km.)
Dense forest	0
Light forest	20.14
Agricultural area	46.97
Bare land	9.99
Plantation area	11.86
Water body	0.77
Total	**89.73**

In 2015, the algorithm created 2015_mean blue information by 100% (<62.71) for the first starting node (Figures 7 and 8). The next two nodes, MSVIT3 < 0.44 and 2015_mean blue < 65.20 were generated. The MSVIT3 (52.2%) was light forest and the other node still divided to dense forest and plantation area with 21.7% and 17.4% of the mean blue information derived in 2015. Moreover, 47.8% of the mean blue was classified to agricultural area and the next one node was classified to body of water and bare land from NIR information in 2015 at 13% and 17.4%, respectively. The largest area class covered was bare land, trending due to deforestation having an area at 48.66 sq.km., followed in decreasing order by dense forest 18.13 sq.km, agricultural area 16.08 sq.km, and body of water 0.29 sq.km, respectively (Table 5).

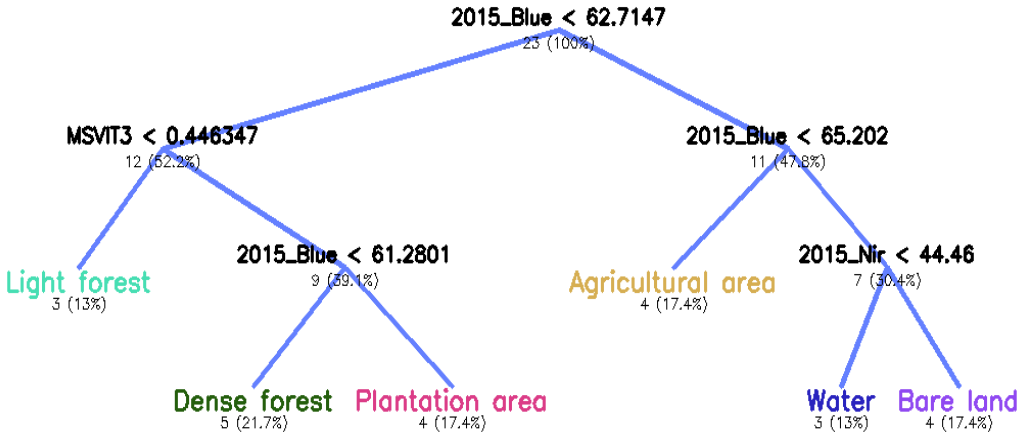

Figure 7. CART parent and child nodes in 2015

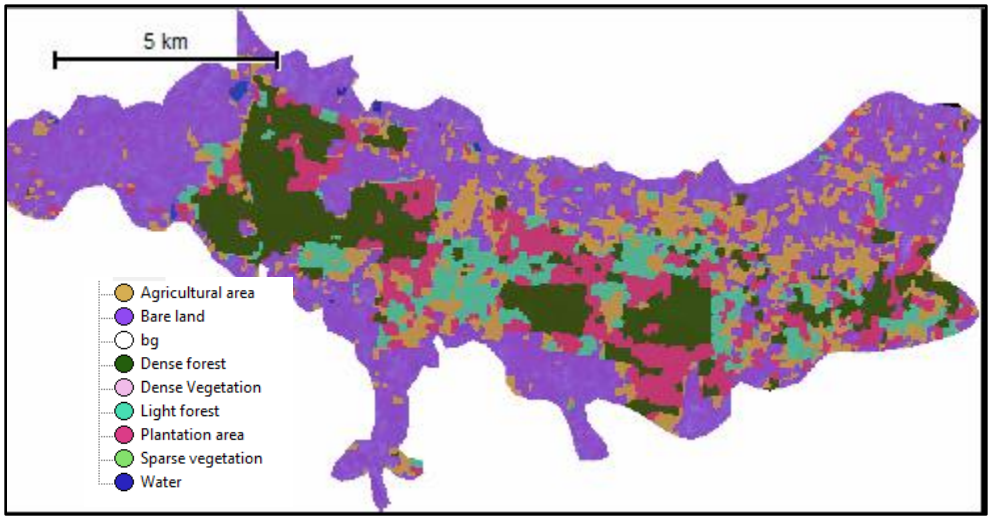

Figure 8. Landsat 7 ETM^{+} imagery classification result in 2015

Table 5. The classification area in 2015

Class names	Area (sq.km.)
Dense forest	18.13
Light forest	9.32
Agricultural area	16.08
Bare land	48.66
Plantation area	14.05
Water body	0.29
Total	**106.53**

3.2 Accuracy assessment

In the accuracy assessment process, the classified maps were compared with reference objects and collected points data from field surveying in Dong Ranang national forest. The reference data were the same data set as the data used as the sample points. These data, derived from 3 acquiring dates, were converted from the point data format to TTA Mask utilizing a process called Error matrix which was based on TTA Mask for performing and comparing with classified images. In 1999, for dense forest, the user accuracy was 85%, for light forest 70%, plantation area 86%, and overall accuracy was 87.33%. Moreover, in 2007, the overall accuracy was 88.17%, the user accuracy for dense forest was 87%, for light forest 71%, and plantation area scored 88%. Lastly, the overall accuracy in 2015 was 89.63%, dense forest had user accuracy of 91%, light forest 46%, plantation area 91%, and agricultural area 8%.

3.3 Change detection

Change detection analysis deployed the image hierarchical image network described above. Image classified by date, date 1 (1999), date 2 (2007) and date 3 (2015) were synchronized to the main map. The main map refers to the output window which the classification images were synchronized to this panel for changes evaluation and perform final discussion approach.

3.4 Map synchronization

Map synchronization is the process used for transferring the classification results in each year to the main map. However, the operation under the eCognition environment is a multi-tasking one in which the analyst can create more than one map. This makes it possible to send results from different maps over different time periods through various processes in order to obtain specific results. For example, this paper used these features to examine LU/LC changes. In addition, under the same environment, data can be analyzed using the same classification rules, which means it is unnecessary to create a new rule set for each satellite image from different specific time frames.

3.5 Image hierarchical network

The synchronized algorithm enabled the transfer of the classified maps to the main map. The classification results for 1999 data were synchronized to the main map. At the same time, on the main map, the data layer L1T1 was copied for creating the upper image object hierarchy network which represented the classification results in 1999. The data layer L1T2 was used to maintain the classification results in 2007. Then, change detection analysis from 1999-2007 was begun by using the relational to sub-objects approach. The results of land use analysis for each period were sent to

the main map. The main map data layer consisted of L1T1 classification results for 1999, L1T2 classification results for 2007, and L1T3 classification results for 2015. These classification results were arranged in the structural relationships of hierarchical image objects in horizontal and vertical aspects. This is called change detection analysis using a subtractive approach. Therefore, the conversion to sub-objects algorithm was used to perform this task, which was to 'cookie-cut' the outlines for the images that had been classified in all 3 periods. After that, the classification results L1T2 (Level_changeT1_T2: 1999-2007) and L1T3 (Level_changeT2_T3: 2007-2015) were copied to the upper layer data.

3.6 Class description creation

In order to evaluate hierarchical network of image objects on changes level, class descriptions were created to define target classes properties, and to analyze changes by defining class definitions and class-related features (relation to sub objects). The top most layer was 2007, and an image object at Level 1 maintaining the first hierarchical relationship with classified data in 1999 (Level 2) shows the vertical distance of the hierarchy image objects. The L2 level related to the level L1, is the lowest level of hierarchical mage object. However, by comparing with overlay analysis derived in GIS, which was not able to draw structure relationships, both horizontal and vertical directions are used as the supporting tools when preparing in the object-based image analysis approach.

The changes layer (Change_level_T1_T2) in 1999 indicated that the image object in the red area was classified as sparse forest after considering the NDVI and MSAVI2 values as described above. This was to evaluate the result of the transition layer in 1999, that is to see if it had changed or not. For example, the sparse forest tree tops can be changed to other land cover types. Changes in land use from light forest in 1999 to 2007 can be determined that it changed if the hierarchical image object distance on the data layer Change_level_T1_T1 related to the image object level L1T1 (2) by the distance = 1 (100%), and associated with L1T2 (1) = 0 (not related). This process is called class description achieved by using class relations to sub object features creating a class description for each target class (Figure 9).

3.7 Change detection analysis in 2007-2015 using relational to sub-objects

At this stage, there were the same conceptual routine tasks concerned with the study of land use changes during 1999-2007. The results from 1999-2007 were input to the top most changes level. The L1T3 layer was duplicated to the sub-object level by performing the subtractive approach to changes image objects. The analytical process that considered the overlapping of two-time series of land use was done by analyzing all cross validation aspects (Figures 10 and 11).

3.8 Land use land cover changes detection

Then, above, we have described the methodology of image classification in each year using CART and LU/LC change detection via the image hierarchical subtractive approach. There were 6 LU/LC classes classified in this area, namely, (1) dense forest, (2) light forest, (3) agricultural area, (4) bare land, (5) plantation area, and (6) body of water. The LU/LC change evaluation from 1999-2007 found that the dense forest showed a dramatically decrease in the area of -13.88 sq.km. The highest increase in area was plantation area (+38.68 sq.km), followed by agricultural area increased +29.43 sq.km, and plantation area increased +38.68 sq.km, respectively. Additionally, the evaluation from 2007-2015 indicated that the most decreased LU/LC class was agricultural area with -30.89 sq.km compared with 1999-2007, followed by the most increasing area which was bare land (+38.67 sq.km), and dense forest showed a slight increase of 18.13 sq.km (Table 6).

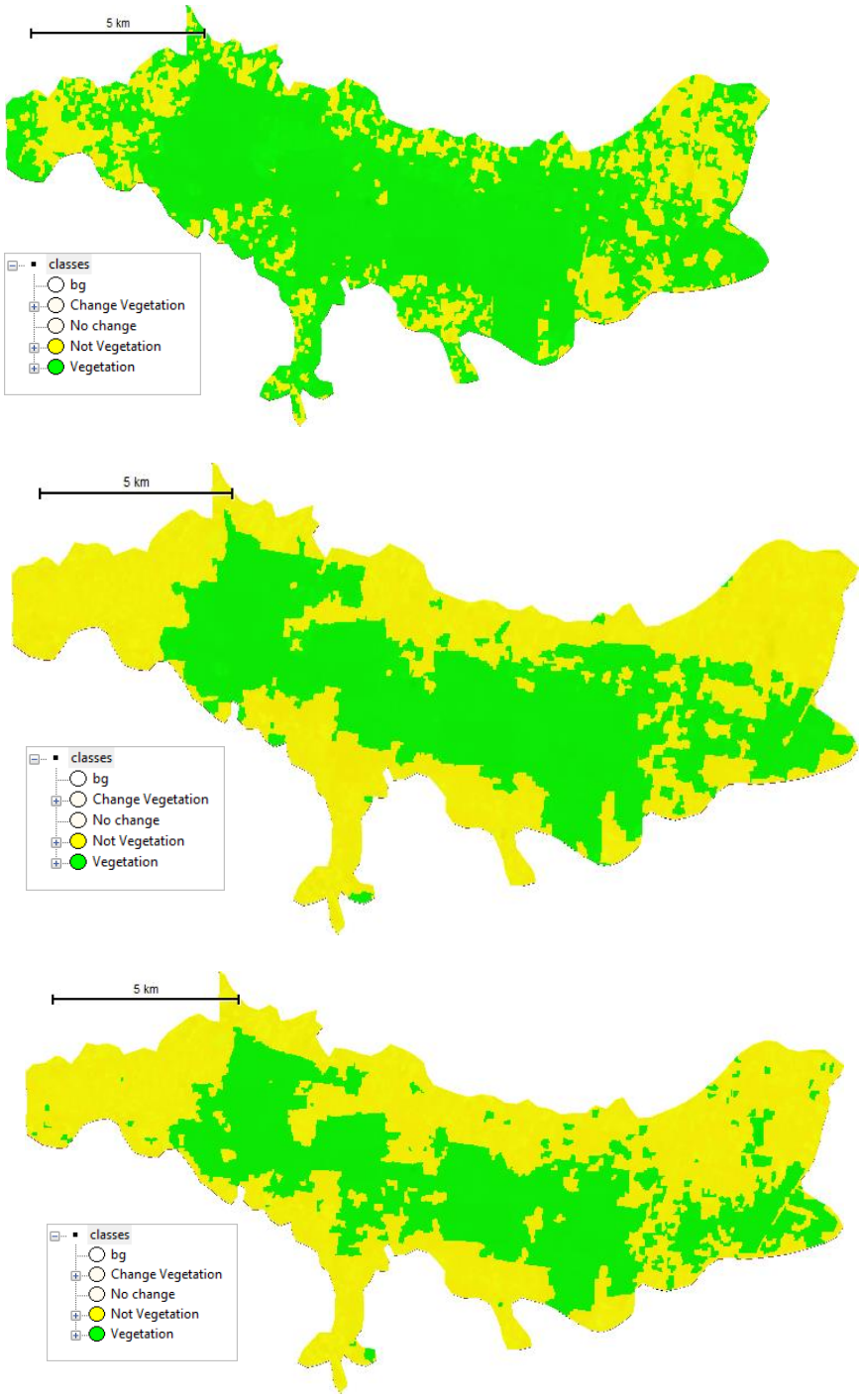

Figure 9. Forest and non-forest areas grouped by corresponding classes (a) 1999, (b) 2007, and (c) 2015

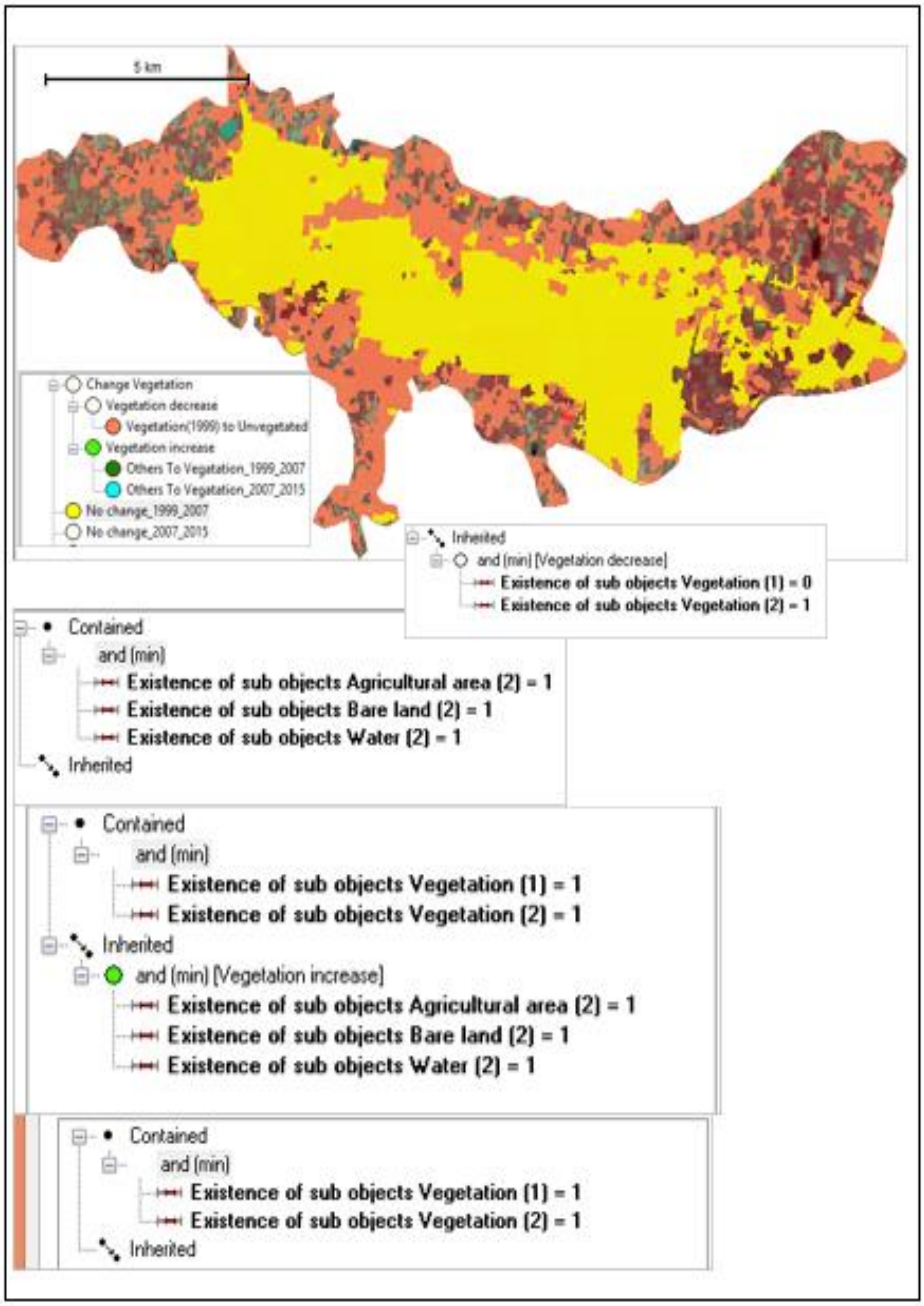

Figure 10. Land use change evaluation using hierarchical image network from 1999-2007

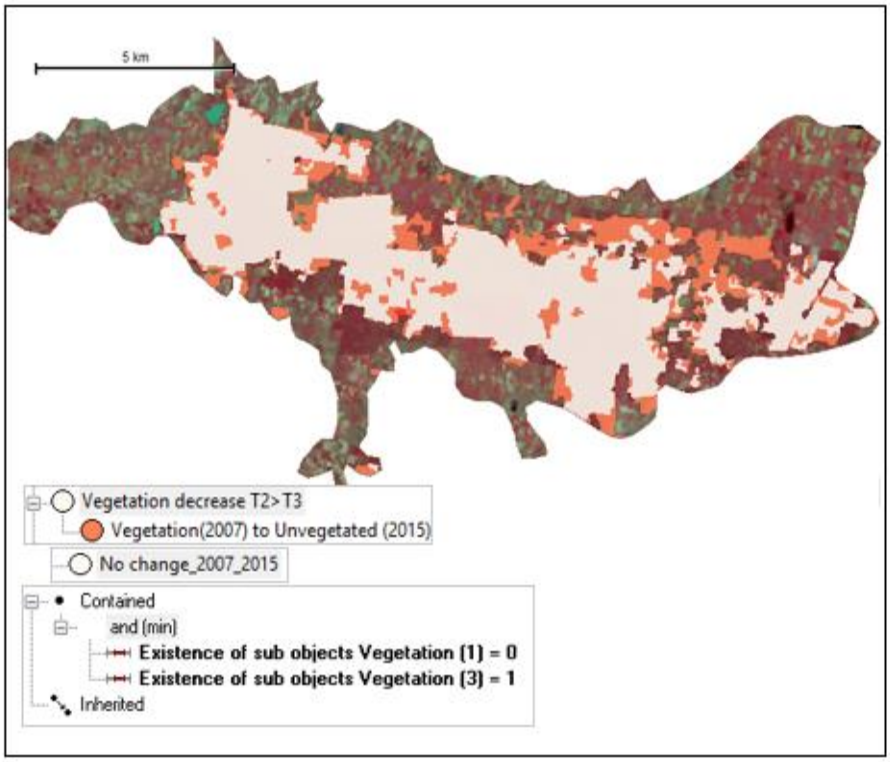

Figure 11. Land use change evaluation by using hierarchical image network from 2007-2015

Table 6. Land use land cover changes in Dong Ranang national forest from 1999-2015

Class name	1999 (km^2)	2007 (km^2	2015 (km^2)	Changing rate from 1999-2007	Changing rate from 2007-2015
Dense forest	13.88	0	18.13	-13.88	+18.13
Light forest	14.70	20.14	9.32	+6.14	-3.18
Agricultural area	17.54	46.97	16.08	+29.43	-30.89
Bare land	5.88	9.99	48.66	-4.11	+38.67
Plantation area	50.57	11.86	14.05	+38.68	+2.19
Water body	4.325	0.77	0.29	-3.555	0.48
Total	**106.89**	**89.73**	**106.53**		

4. Conclusions

This paper identifies forest changes in Dong Ranang National Forest using object-based image analysis applying CART classifier to classify images from the three-time series of LANDSAT 7 ETM^+, namely 1999, 2007, and 2015. The data of these images underwent image pre-processing in order to import to the object-oriented analytical tool effectively.

The LANDSAT 7 ETM$^+$ images from 1999-2007 were used for LU/LC changes detection analysis. Each image was classified individually using CART, including the integration of sampling points that represented LU/LC classes derived from visual interpretation. The classification stratification was composed of six classes, namely, (1) dense forest (2) light forest (3) agricultural lands (4) bare land (5) plantation this area, and (6) body of water. Under the object-oriented environment tool, the classification rule set was defined for the classification of processes using Cognition Network Language (CNL). This is consistent with image object properties and inherited information from image segmentation process. The segmentation process begins with pixel values, which are used to create image objects, each of which has its own reflectance properties, such as mean values of chosen bands, including spatial information among image objects. To increase the accuracy of the classification effectively, CART algorithm was used for classifying the three dates of Landsat imageries. In order to achieve the appropriation of the classification results, the processes began with vector sampling in order to train the data. These samples were brought into the process as the training data, creating LU/LC classes representative from known to uncertain classes. The vector to sample approach comprises training, applying and querying. The training is a process that lets the system know that the user has now determined that the selected sample is the data set used for the classification. The system assesses the various statistical correlations that were selected with the characteristics of the data that has been used. Applying CART is the process by which the selected tool is completely used in the system, the last step that analysts have chosen. Query decision tree making is a rendering process of tree network to show the results of the selection of factors responding to selection for use in satellite image analysis. The branches showed the diagram of the proportion of each selected classification factor.

Accuracy assessment was performed separately by year. The reference data obtained from the point data was derived from visual interpretation. After importing point sample data, the researchers exported the image objects that had been classified by visual interpretation, and then converted from sample point data into TTA mask used for comparing classified image objects with correct reference data. The overall accuracy in 1999 was 87.33%, in 2007 was 88.17% and in 2015 was 89.63, respectively.

Change detection in Dong Ranang National forest deployed an object-oriented image analysis for classifying the 3 time series described above. The results indicated that the forest area in 1999 was still abundant, and spread over the whole area with a total forest area of 79.15 sq.km. Some vegetation indices were used for image classification, including class description and image object hierarchical network. In 2007, the forest area had decreased significantly, and showed an area of 32 sq.km, which was a drop of 47.15 sq.km from 1999. More interestingly, the 2007 data showed that some areas of forest had changed to unexpected area type. It was found that the agricultural area covered an area of 46.97 sq.km in 2015. The forest area had still not rebounded significantly. In 2007, most of this area was still empty spaces, which was because forest area had changed to bare land. However, the Office of Forest Resources Management No. 7 (Khon Kaen province-based office) has developed reforestation projects aimed at restoring the state of the forest, which had been over exploited.

5. Acknowledgements

I would like to express gratitude to Geoinformatics Research Unit, Faculty of Informatics, Mahasarakham University for the research fund support.

References

[1] Blaschke, T., 2013. Object based image analysis: a new paradigm in remote sensing? *American Society for Photogrammetry and Remote Sensing Annual Conference*, March, 2013, 24-28.

[2] Lang, S., 2008. Object-based image analysis for remote sensing applications: modeling reality - dealing with complexity. In: T. Blaschke, S. Lang and G.J. Hay, eds. Object-Based Image Analysis: Spatial Concepts for Knowledge-Driven Remote Sensing Applications. Heidelberg: Springer; pp. 3-27.

[3] Karimi, H., Jafarnezhad, J. and Kakhani, A., 2020. Landsat time-series for land use change detection using support vector machine: Case study of Javanrud District, Iran. In: *2020 International Conference on Computer Science and Software Engineering (CSASE)*, 2020. 12831.

[4] Martha, T.R., Kerle, N., van Westen, C.J., Jetten, V. and Kumar, K.V., 2011. Segment optimization and data-driven thresholding for knowledge-based landslide detection by object-based image analysis. *IEEE Transactions on Geoscience and Remote Sensing*, 49(12), 4928-4943.

[5] Heumann, B.W., 2011. An object-based classification of mangroves using a hybrid decision tree-support vector machine approach. *Remote Sensing*, 3(11), 2440-2460.

[6] Hussain, M., Chen, D., Cheng, A., Wei, H. and Stanley, D., 2013. Change detection from remotely sensed images: From pixel-based to object-based approaches. *ISPRS Journal of Photogrammetry and Remote Sensing*, 80, 91-106.

[7] Ma, C., Ai, B., Zhao, J., Xu, X. and Huang, W., 2019. Change detection of mangrove forests in coastal Guangdong during the past three decades based on remote sensing data. *Remote Sensing*, 11(8), 921, https://doi.org/10.3390/rs11080921 https://doi.org/10.3390/rs11080921

[8] Liu, X., Chen, Y., Li, S., Cheng, L. and Li, M., 2019. Hierarchical classification of urban ALS data by using geometry and intensity information. *Sensors*, 19(20), 4583, https://doi.org/ 10.3390/s19204583

[9] Song, A., Kim, Y. and Han, Y. 2020. Uncertainty analysis for object-based change detection in very high-resolution satellite images using deep learning network. *Remote Sensing*, 12(15), 2345, https://doi.org/10.3390/rs12152345

[10] Pereira-Pires, J.E., Aubard, V., Silva, J.M.N., Ribeiro, R.A., Pereira, J.M.C., Fonseca, J.M. and Andre, M., 2020. Pixel-based and object-based change detection methods for assessing fuel break maintenance. In: *2020 International Young Engineers Forum (YEF-ECE)*, July, 2020, 49-54.

[11] Drăguţ, L., Eisank, C. and Strasser, T., 2011. Local variance for multi-scale analysis in geomorphometry. *Geomorphology*, 130(3), 162-172.

[12] Qin, R., Huang, X., Gruen, A. and Schmitt, G., 2015. Object-based 3-D building change detection on multitemporal stereo images. *IEEE Journal of Selected Topics in Applied Earth Observations and Remote Sensing*, 8(5), 2125-2137.

[13] Zhang, H., Eziz, A., Xiao, J., Tao, S., Wang, S., Tang, Z., Zhu, J. and Fang, J., 2019. High-resolution vegetation mapping using extreme gradient boosting based on extensive features. *Remote Sensing*, 11(12), 1505, https://doi.org/10.3390/rs11121505

[14] Qi, J., Chehbouni, A., Huete, A.R., Kerr, Y.H. and Sorooshian, S. 1994. A modified soil adjusted vegetation index. *Remote Sensing of Environment*, 48(2), 119, https//doi.org/10.1016/0034-4257(94)90134-1

[15] Ren, H. and Feng, G., 2014. Are soil-adjusted vegetation indices better than soil-unadjusted vegetation indices for above-ground green biomass estimation in arid and semi-arid grasslands? *Grass and Forage Science*, 70(4), https//:doi.org/10.1111/gfs.12152

[16] Huo, L.-Z., Boschetti, L. and Sparks, A.M., 2019. Object-based classification of forest disturbance types in the conterminous United States. *Remote Sensing*, 11(5), 477, https://doi.org/10.3390/rs11050477

[17] Zhan, Q., Molenaar, M. and Tempfli, K., 2002. Hierarchical image object-based structural analysis toward urban land use classification using high-resolution imagery and airborne LIDAR data. In: *Proceedings of the 3rd International Symposium on Remote Sensing of Urban Area's 2002*, pp. 251-258.

[18] Shao, Y. and Lunetta, R.S. 2012. Comparison of support vector machine, neural network, and CART algorithms for the land-cover classification using limited training data points. ISPRS *Journal of Photogrammetry and Remote Sensing*, 70, 78-87.

[19] Denison, D.G.T., Mallick, B.K. and Smith, A.F.M., 1998. A Bayesian CART algorithm | *Biometrika*, 85(2), 363-377.

[20] Ma, H., Liu, Y., Ren, Y., Wang. D., Yu, L. and Yu, J., 2020. Improved CNN classification method for groups of buildings damaged by earthquake, based on high resolution remote sensing images. *Remote Sensing*, 12(2), 260, https//doi.org/10.3390/rs12020260

[21] Hong, L. and Zhang, M., 2020. Object-oriented multiscale deep features for hyperspectral image classification. *International Journal of Remote Sensing*, 41(14), 5549-5572.

[22] Rahimizadeh, N., Kafaky, S.B., Sahebi, M.R. and Mataji, A. 2019. Forest structure parameter extraction using SPOT-7 satellite data by object- and pixel-based classification methods. *Environmental Monitoring and Assessment*, 192(1), 43, https://doi.org/10.1007/s10661-019-8015-x

[23] Fallatah, A., Jones, S. and Mitchell, D. 2020. Object-based random forest classification for informal settlements identification in the Middle East: Jeddah a case study. *International Journal of Remote Sensing*, 41(11), 4421-445.

[24] Ghasemain, B., Asl, D.T., Pham, B.T., Avand, M., Nguyen, H.D. and Janizadeh, S., 2020. Shallow landslide susceptibility mapping: A comparison between classification and regression tree and reduced error pruning tree algorithms. *Vietnam Journal of Earth Sciences*, 42(3), 208-227.

[25] Benedetti, A., Picchiani, M., Del Frate, F., 2018. Sentinel-1 and sentinel-2 data fusion for urban change detection. *IGARSS 2018-2018 IEEE International Geoscience and Remote Sensing Symposium*, Valencia, 2018, 1962-1965.

[26] Lin, Y., Zhang, L., Wang, N., Zhang, X., Cen, Y. and Sun, X., 2020. A change detection method using spatial-temporal-spectral information from Landsat images. *International Journal of Remote Sensing*, 41(2), 772-793.

[27] Ai, J., Zhang, C., Chen, L. and Li, D., 2020. Mapping annual land use and land cover changes in the Yangtze estuary region using an object-based classification framework and landsat time series data. *Sustainability*, 12(2), 659, https://doi.org/10.3390/su12020659

[28] Zhang, X., Xiao, P. and Feng, X. 2020. Object-specific optimization of hierarchical multiscale segmentations for high-spatial resolution remote sensing images. *ISPRS Journal of Photogrammetry and Remote Sensing*, 159, 308-321.

[29] Krauß, T. and Tian, J., 2020. Automatic change detection from high-resolution satellite imagery. In: D.G. Hadjimitsis, K. Themistocleous, B. Cuca, A. Agapiou, V. Lysandrou, R. Lasaponara, N. Masini and G. Schreier, eds. *Remote Sensing for Archaeology and Cultural Landscapes: Best Practices and Perspectives Across Europe and the Middle East*. Cham: Springer International Publishing, pp. 47-58.

[30] Ghosh, D. and Chakravortty, S., 2020. Change detection of tropical mangrove ecosystem with subpixel classification of time series hyperspectral imagery. In: D.J. Hemanth, ed. *Artificial Intelligence Techniques for Satellite Image Analysis*. Cham: Springer International Publishing, pp. 189-211.

[31] Tejenaki, S.A., Ebadi, H. and Mohammadzadeh, A. 2020. Automatic road detection and extraction from MultiSpectral images using a new hierarchical object-based method. *Journal of Geomatics Science and Technology*, 9(3), 13-27.